Biointerface Research in Applied Chemistry
Platinum Open Access Journal (ISSN: 2069-5837)

Article
Volume 12, Issue 4, 2022, 5116 - 5130
https://doi.org/10.33263/BRIAC124.51165130

Eco-Friendly Approach to Corrosion Inhibition of Copper in HNO_3 Solution by the Expired Tylosin Drug

Mahmoud A. Ali [1], Abdelfattah M. Ouf [1], Ahmed El-Hossiany [1,2], Abd El-Aziz S. Fouda [1,*]

[1] Department of Chemistry, Faculty of Science, El-Mansoura University, Egypt; asfouda@mans.edu.eg (A.E.-A.S.F.);
[2] Delta for Fertilizers and Chemical Industries, Talkha, Dakahleya, 1179 Egypt; dr.ahmedselm@gmail.com (A. E.-H.);
* Correspondence: asfouda@mans.edu.eg (A.E.-A.S.F.);

Scopus Author ID 56231506400

Received: 4.07.2021; Revised: 15.09.2021; Accepted: 20.09.2021; Published: 17.10.2021

Abstract: Expired Tylosin Drug (ETD) is examined as corrosion inhibitor for copper (Cu) dipped in 2.0 M HNO_3. The study was conducted utilizing ac impedance spectroscopy (EIS), weight loss (WL), polarization, and surface checks to illustrate the importance of this ETD to prevent the corrosion process for Cu. The influence of temperature and concentration of ETD on the efficiency of inhibition were tested. The corrosion mechanism occurs when the ETD molecules block the active center in the electrode surface. Langmuir isotherm is the isotherm that is applied in the process of adsorption. The effect of temperature at various temperatures on the corrosion efficiency was investigated in case of the presence and absence of ETD. Finally, thermodynamic parameters for the inhibition process were determined. Results were of all methods used are in good agreement.

Keywords: corrosion; inhibition; Langmuir isotherm; copper; ETD; EIS.

1. Introduction

Copper is a relatively noble metal that does not corrode readily in acids unless some oxidizing agents or oxygen is present. For that reason, it is broadly used in the manufacturing of electrical conductors, thermal exchangers, and electronics [1–2]. To fabricate electronic components, copper must be dissolved in aggressive solutions and be electroplated. Some electronic components like printed circuit boards must be treated with corrosive solutions during fabrication to remove scales. Nitric acid is one of the aggressive solutions frequently used in various industries [3]. There are many methods of controlling and preventing corrosion. The use of corrosion inhibitors is the most common [4]. Corrosion inhibitors have been used since the 19th century; they work by adsorption of ions or molecules on a metal surface [5]. Scientists are ever in search of novel, efficient, and economical corrosion inhibitors species to minimize corrosion [6]. Recently, some authors examined the inhibiting action of drugs such as (Table 1):

Table 1. Some expired drugs utilized as corrosion inhibitors for Cu in acidic media.

Sample	Inhibitor (drug)	Medium	% IE	References
Copper	Losartan Potassium (LP)	H_2SO_4	91.2	[7]
Copper	Meropenem	HCl	87.6	[8]
Copper	Cefpirome	H_2SO_4	91.9	[9]
Copper	Streptoquin	HCl	83.1	[10]

It was proved by the earlier researchers that organic molecules bearing hetero atoms like N, O, S, etc., and containing aromatic rings act as good corrosion protecting molecules.

The aim of the current work is to study the impact of expired Tylosin as a new compound on the inhibition of copper corrosion in 2 N HNO_3 solutions. In our investigation, we used the chemical method (gravimetric method), electrochemical practices (potentiodynamic polarization and electrochemical impedance spectroscopy) in addition to studying the metal surface by AFM, FT-IR- and XPS.

2. Materials and Methods

2.1. Components of sampling materials.

Table 2. Chemical analysis of the components (wt. %) of Cu.

Element	Sn	Fe	Ag	Bi	Pb	As	Cu
Wt %	0.001	0.01	0.001	0.005	0.002	0.0002	The rest

2.2. Solutions.

2M nitric acid (HNO_3) was prepared in the laboratory by diluting the appropriate volume of analytical grade, 69% HNO_3, with bi-distilled water. Using the prepared HNO_3, different solutions containing 2.0 M HNO_3 were prepared without or by adding different concentrations of ETD ranging from 50 to 300 ppm. By liquefying an appropriate mass of the ETD (1.0 g) in a specified volume of bi-distilled water, 1000 ml stock solutions (1000 ppm) of the examined ETD were created (1.0 L). By liquefying the stock ETD and employing an aggressive solution, the tested dosages ranging from (50–300 ppm) were prepared.

2.3. Inhibitor.

ETD is a pharmaceutical chemical that is easily soluble in water, has a higher molecular weight, contains numerous donating atoms (N and O), is readily available as a medicinal medicine, is non-toxic, and has the following structure:

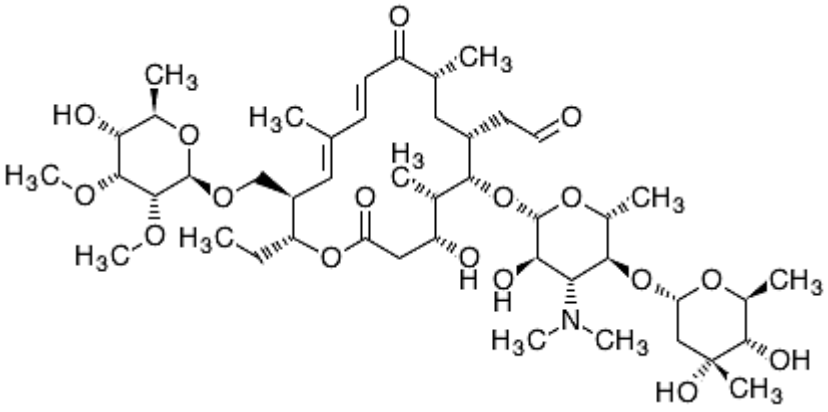

Chemical Formula: $C_{46}H_{77}NO_{17}$
Molecular weight: 916.112 g·mol^{-1}

Figure 1. Molecular structure of ETD.

2.4. Weight loss (WL) measurements.

The WL is used to investigate the dissolution of Cu in a fresh solution of 2.0 M HNO_3 and the absence of ETD dose changes. Seven samples are cut and sanded the same way as before, then washed in double distilled water, dried, and weighed (w^o). WL measurements were taken by dipping the sheet in 100 ml of aggressive medium with and without various dosages (50 to 300 ppm) of the ETD for 180 minutes at a temperature range of 25-40^{o}C. At 30-minute

intervals, the samples were taken from the test solution, submerged in water, dried, and reweighed (w). (IE%) and the degree of Cu coverage (θ) have been computed by the balance:

$$\%IE = \theta \times 100 = \left(\frac{W^{o}-W}{W^{o}}\right) \times 100 \quad (1)$$

where, w and w° refer to the WL of Cu per unit area in the attendance and absence of the examined ETD, consistently. The corrosion rate (C.R) was dignified from:

$$C.R = \Delta W/A.t \quad (2)$$

where, WL (mg) is ΔW, the sample surface area exposed to the solution in cm^2 expressed by A, and the submersion time as t in min.

2. 5. Potentiodynamic polarization (PP) tests.

The potentiodynamic tests were utilized through a cell consisting of three classic electrodes, the working electrode studied. This electrode is made of Cu metal, and the surface area exposed in it is 1 cm^2. Before utilizing the electrode, it is processed according to the tested following WL. The working electrode is employed in the solution utilized at the OCP for 30 minutes, where the stability condition is obtained. Polarization bends were confirmed at a steady scan rate of 0.5 mVs^{-1} initially from 0.35 V to -1.3 V (SCE) [11, 12]. In this test, the current density is a function of the calculation. Experiments are repeated three times to confirm them". The IE% enabled for ETD is as bellow balance:

$$\%IE_{p} = \theta \times 100 = \left(\frac{i^{o}_{corr} - i_{corr}}{i^{o}_{corr}}\right) \times 100 \quad (3)$$

where i^{o}_{corr} and i_{corr} are the uninhibited and inhibited corrosion current density data, individually.

2.6. AC impedance spectroscopy (EIS) test.

EIS conducted the experiment by utilizing AC signals with amplitudes ranging from 100 kHz to 100 mHz and peaks of 5 mV at OCP. Using the Gamry Echem software and the charge transfer resistance (R_{ct}) as a function of significant the value of protection, all of the impedance results were compatible with the suitable equivalent circuit [13].

$$\%IE_{EIS} = \theta \times 100 = \left(\frac{R_{ct} - R^{\circ}_{ct}}{R_{ct}}\right) \times 100 \quad (4)$$

where R_{ct} and R_{ct}° are the resistances for the inhibited and the inhibitor-free system from ETD. In the electrochemical examination, the device utilized in the EIS tests was Gamry includes DC105 DC Corrosion Program and EIS300 EIS program, as well as a computer for data collection. Echem Analyst type 5.5 was utilized to plot, estimate, and synthesize data. All electrochemical educations were useful at 25 °C.

2.7. Morphology of the surface.

2.7.1 Atomic force microscopy (AFM).

AFM is a specialized test that provides information on the surface of a Cu sample with metric linear purity. Persecution is used to execute and appraise measured knowledge. From the computer code for SPM management [14].

2.7.2. Attenuated total reflection Infra-Red (ATR-IR).

The FTIR-Spectrometer iS 10 was used to register FT-IR spectra in the spectral range 4000 to 500 cm^{-1} using the Attenuated Total Reflectance (ATR) approach (Thermo Fisher Scientific, USA). After inhibitor adsorption, an FT-IR spectrum is a useful tool for comparing inhibitor and corrosion products. After a 24-hour immersion in the FT-IR, the peak values for ETD and Cu were recorded in the acid corrosive environment with 300 ppm of *ETD* [15].

2.7.3. X-ray spectroscopy (XPS) examination.

The morphology of Cu metal samples was evaluated using an electronic X-ray spectroscopy (XPS) equipment ESCALAB 250Xi, Thermo-Scientific, USA, before and after being immersed in a solution of 2 M nitric acid in the presence and absence of ETD (300 ppm) for 24 hours. This method entails, Cu coupons were handled the same way as previous treatment coupons were cured for Wl practice.

3. Results and Discussion

3.1. WL tests.

WL measurements of Cu samples were reported after Altered interval time of dipping (30, 60, 90, 120,150 and180 min) at various temperatures (25, 30, 35, 40°C), WL graph at 25°C is shown in Figure 1. The percent IE data at various temperatures is shown in Table 3. The results showed that when ETD was added to the Cu samples, the C.R of the Cu samples decreased in a 2M nitric acid solution. When the ETD dose was increased, the IE percent increased as well. The graphs are virtually linear, indicating that all molecules introduced in the measured concentration range find a free surface site to adsorb on. As a result, each additional molecule plays a direct role in the inhibitory activity. As a result of the Cu-covered surface area, the percent IE grows as the ETD dose improves.

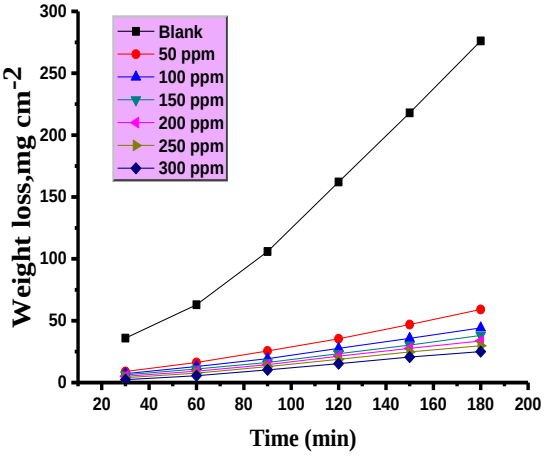

Figure 2. WL-time diagrams for the liquefaction of Cu in the attendance and absence of altered dose of ETD at 25◦C.

Table 3. The temperatures influence C.R. and %IE of Cu in an acidic environment in the existence and absence of altered dose of ETD.

Temperature °C	[inh] ppm	C.R. (mg cm^{-2} min^{-1})	% IE
25	50	0.24459	82.4
	100	0.17567	87.4
	150	0.14459	89.6
	200	0.11756	91.6
	250	0.10405	92.5
	300	0.08243	94.1
30	50	0.47564	75.7
	100	0.38228	80.4
	150	0.31615	83.8
	200	0.2967	84.8
	250	0.26169	86.6
	300	0.20334	89.6
35	50	0.56781	71.3
	100	0.44527	77.5
	150	0.39389	80.1
	200	0.38203	80.7
	250	0.32867	83.4
	300	0.26555	86.6
40	50	0.68352	67.1
	100	0.56293	72.9
	150	0.45898	77.9
	200	0.45482	78.1
	250	0.41116	80.2
	300	0.34671	83.3

3.2. The isotherm in adsorption process.

The adsorption isotherm was used to explain the reaction that happened between the Cu surface and the ETD. The adsorption of the ETD molecule on the Cu surface is thought to have risen as the inhibitor dose was raised. It is also assumed that the adsorption of the investigated ETD occurs in a monolayer so that the adsorption process obeys the Langmuir isotherm. The following equation is used to investigate the adsorption mechanism:

$$\frac{C_{\text{inh}}}{\theta} = \frac{1}{K_{\text{ads}}} + C_{\text{inh}} \qquad (6)$$

where C refers to the dose of ETD in the electrolyte, and kads signifies the equilibrium constant for the procedure of adsorption. Commonly, the C.R of Cu in an acidic environment improved with the raising in temperature. The ΔG°ads tests at all measured temperatures can be obtained from the next balance [16]:

$$K_{\text{ads}} = \left(\frac{1}{55.5}\right) \exp\left(\frac{-\Delta G^{\Theta}_{\text{ads}}}{RT}\right) \qquad (7)$$

where 55.5 refers to the dose of water in (M) at the interface among Cu/solution. ΔH°ads dignified by the balance (8) which is distinct as Van't Hoff [17]:

$$\lg K_{\text{ads}} = \frac{-\Delta H^{\Theta}_{\text{ads}}}{2.303RT} + \text{constant} \qquad (8)$$

The heat of adsorption (ΔH°ads) was computed by drawing log kads against 1/T as drawn in Figure 4. The slope of the line equals (-ΔH° ads/R). Then by applying the following balance [18]:

$$\Delta S^{\Theta}{}_{\text{ads}} = \frac{\Delta H^{\Theta}_{\text{ads}} - \Delta G^{\Theta}_{\text{ads}}}{T} \qquad (9)$$

From the values of $\Delta G°_{ads}$ and $\Delta H°_{ads}$ in equation (9), $\Delta S°_{ads}$ data were obtained at all examined temperatures. In Table 4, resolute thermodynamic tests for the studied ETD on Cu surface in a 2.0 M nitric acid environment were testified. $\Delta G°_{ads}$ data of the table confirm the spontaneous adsorption of ETD on the Cu surface, through the negative values obtained free energy, whose negative value losses with improving temperature, which confirms that the adsorbed layer is more stable at low temperatures [19, 20]. We know that the data acquired from free energy corroborate that the type of adsorption incidence is physical adsorption, not chemical adsorption, because negative values less than 20 kJ mol^{-1} are known to be physical adsorption, and this matches the results obtained. These findings show that physical adsorption is the dominant mode of adsorption [21-23]. ΔH^{o}_{ads} data obtained from measurements of less than 100 kJ mol^{-1} indicates that the adsorption type is physisorption. The exothermic character is explained by the negative indications of ΔH^{o}_{ads} values when the ETD is added. In the event of appending the ETD, the entropy of adsorption, $\Delta S°_{ads}$, is negative and tiny, which is associated with an exothermic operation [24].

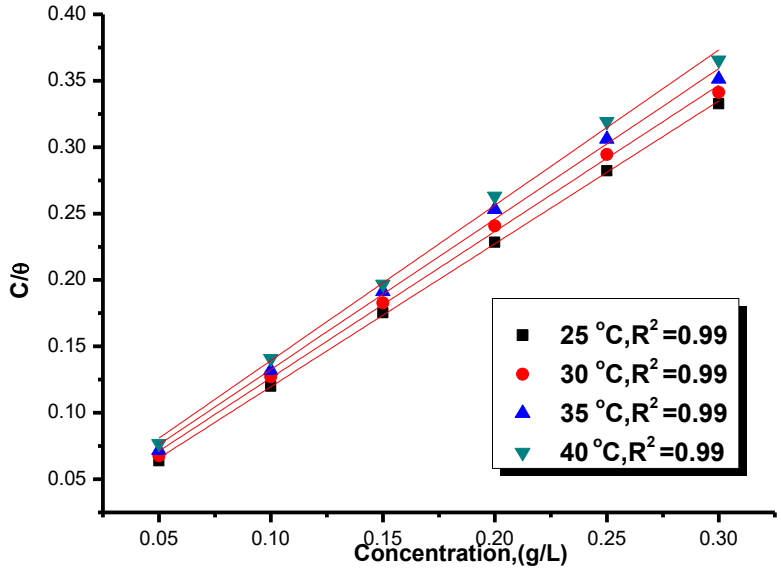

Figure 3. Bends of Langmuir adsorption of Cu in the nonexistence and existence of altered doses of ETD.

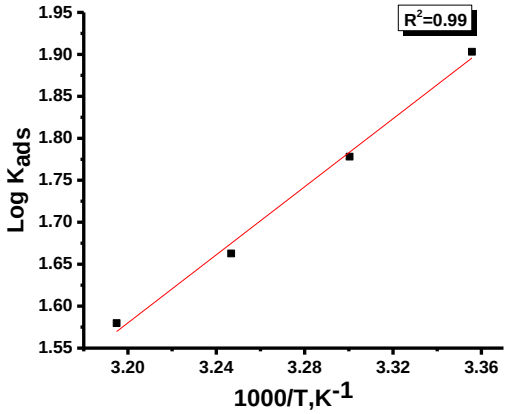

Figure 4. Drawn of log K_{ads} vs 1000/T for the adsorption of ETD on Cu in 2M HNO_3.

Table 4. Parameters of Langmuir adsorption for adsorption of ETD on the Cu surface at altered temperatures.

Temperature °C	$K_{ads}x10^3$ M^{-1}	$-\Delta G^{o}_{ads}$ kJ mol^{-1}	$-\Delta H^{o}_{ads}$ kJ mol^{-1}	$-\Delta S^{o}_{ads}$ J mol^{-1} K^{-1}
25	80	20.8	38	69.7
30	60	20.4		67.3
35	46	20.1		65.1
40	38	19.9		63.5

3.3. The temperature effect on the adsorption process.

The impact of temperature on the Cu dissolution in 2.0 M HNO_3 environment in case of no addition and addition of an altered dose of the ETD was investigated at altered temperatures (25, 30, 35, and 40 ^oC) by WL test in Table 3. The greater the temperature, the higher the C.R, and the lower the IE percent of the ETD. These values are presented in Table 3. The WL test was carried out at four different temperatures to determine if the ETD adsorption on the surface of Cu is chemical or physical. The effect of temperature on the corrosion of Cu pieces employed in the study and dipped in 2M nitric acid was investigated in the presence and absence of varied ETD dosages. In contrast to the C.R., it has been discovered that raising the dose from 50 ppm to 300 ppm increases the rate of protection. The percent IE will decrease as the aggressive environment's temperature rises, but there is a direct correlation between C.R and temperature. The activation energy can be determined using the Arrhenius equation:

$$\log k_{\text{corr}} = \left(\frac{-E_a^*}{2.303RT}\right) + \log A \qquad (10)$$

where E_a^* is the activation of energy of Cu in aggressive environment presence and absence ETD, "and A was utilized for the term exponential factor of Arrhenius. Plots of log k_{corr} versus (1/T) for Cu in 2M nitric acid existence and absence altered doses of ETD exists graphically in Figure 5, which gives straight lines and the calculated data of E_a^* from the slopes of straight lines data that equal ($-E^*_a$ /2.303R) are recognized in Table 5. E^*_a improves with raising doses of ETD representative that the energy barrier for the corrosion reaction raised, also demonstrating that the adsorption of ETD molecules on Cu surface is physical". The (ΔS^*, ΔH^*) measured from the theory of transition state by applied the next balance [25]:

$$k_{\text{corr}} = \left(\frac{RT}{Nh}\right) \exp\left(\frac{\Delta S^*}{R}\right) \exp\left(\frac{-\Delta H^*}{RT}\right) \qquad (11)$$

A drawn of log (k_{corr}/T) versus (1/T) also gave straight lines as appeared in Figure 6, for Cu dissolution in 2M of HNO_3 in the existence and absence of altered doses of ETD. "Slopes from the shape are utilized to measure enthalpy ($-\Delta H^*_a$/2.303R), and the activation entropy of the shape is measured utilizing intersections of the lines [log(R/Nh) $+\Delta S^*_a$/2.303R]. The data of these parameters ($\Delta H^*$and ΔS^*) are verified in Table 5. The ΔH^* reflected endothermic procedure. The calculated values of ΔS^* attendance and absence of ETD are large and negative; this indicates that the activated complex in the rate-determining step prefers association better than dissociation step".

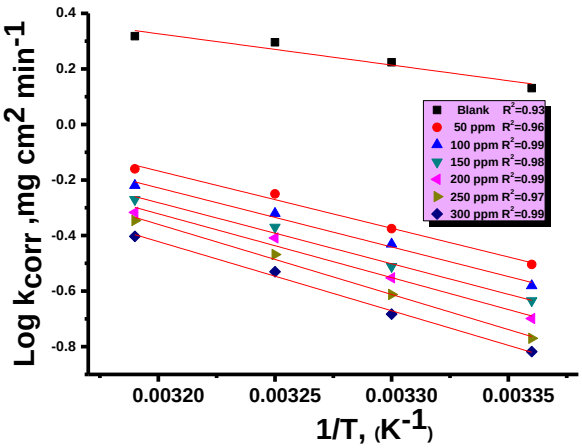

Figure 4. Arrhenius diagram (log k_{corr} vs. 1/ T) for dissolution of Cu in 2M nitric acid without and with the change of ETD.

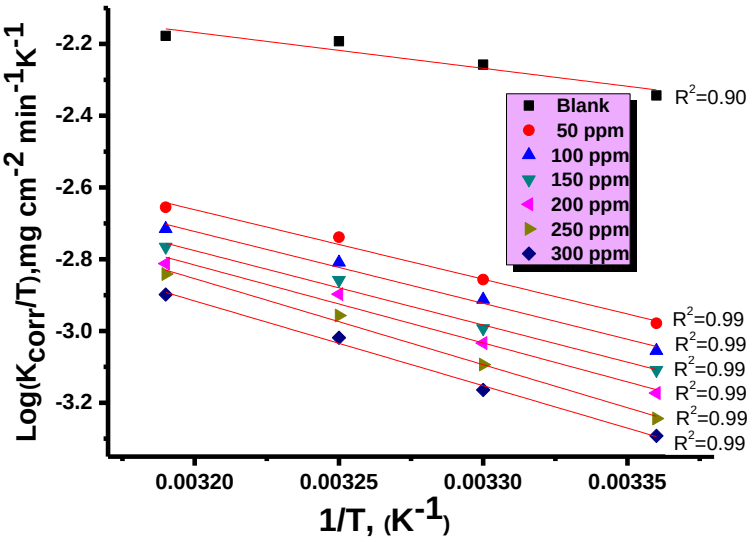

Figure 5. log k_{corr} / T vs. (1/ T) for dissolution of Cu in 2M nitric acid without and with the change of ETD.

Table 5. E^*_a, ΔH^* and ΔS^*data for dissolution of Cu in 2M nitric acid without and with the change of ETD.

[C_{inh}] (ppm)	Ea* kJ mol^{-1}	ΔH* kJ mol^{-1}	-ΔS* J mol^{-1} K^{-1}
0	21.6	19.2	177
50	39.5	37.1	129
100	40.8	38.3	126
150	42.1	39.7	123
200	44.0	41.6	118
250	48.4	45.9	105
300	47.7	45.2	108

3.4. PP tests.

Potentiodynamic bends of Cu in 2.0 M nitric acid in the existence and absence of altered dose of the ETD at 25ºC are displayed in Figure 6. From Figure 6, we see that both cathodic and (Cu dissolution) anodic reactions were inhibited by appending an altered dose of ETD. Both β_a and β_c were shifted to positive and negative directions, correspondingly. The electrochemical parameters, E_{corr}, β_a, and β_c, θ, IE% and i_{corr} were determined and given in Table 6. Data demonstrates that by appending ETD, the data of i_{corr} were lowered while the values of E_{corr} and β_a and β_c had no significant change" [26, 27]. So, the ETD performance is as a mixed kind inhibitor.

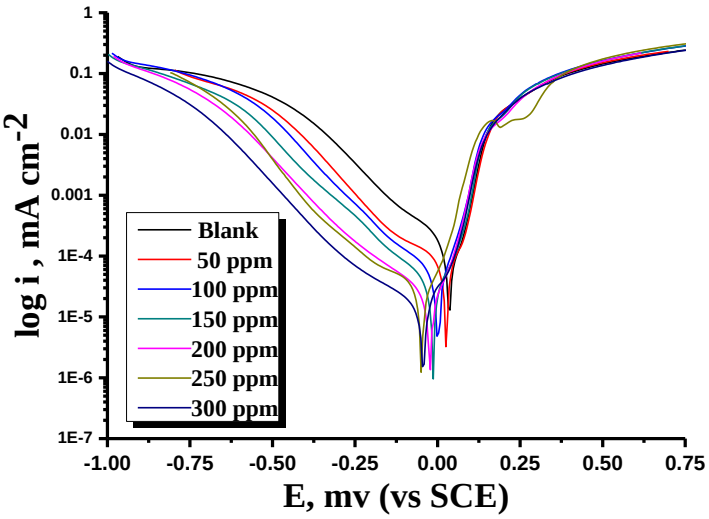

Figure 6. PP bends for the Cu dissolution in 2.0 M nitric acid in existence and nonexistence of altered dose of ETD at 25ºC.

Table 6. Electrochemical parameter, i_{corr}, E_{corr}, β_a, β_c, k_{corr}, θ and IE% of Cu in 2M HNO_3 with an altered dose of ETD.

[C_{inh}] (ppm)	i_{corr}, µA cm^{-2}	-E_{corr}, mV vs SCE	βa, mV dec^{-1}	βc, mV dec^{-1}	C.R mmy^{-1}	θ	%IE
2 M HNO_3	227	35	101	225	107	--	--
50	73	23	95	184	74	0.678	67.8
100	57	13	94	201	59	0.749	74.9
150	37	11	84	195	51	0.837	83.7
200	29	12	89	198	42	0.872	87.2
250	22	15	95	187	34	0.903	90.3
300	18	16	92	192	20	0.921	92.1

3.5. AC impedance spectra (EIS) tests.

Nyquist bends gotten from the Cu at potentials after 30 min dipping in 2.0 M nitric acid in the addition and non-addition of dissimilar dose of ETD. The figure shows the attained Nyquist and Bode, which are drowning in Figures 8 & 9. A semicircle loop is used to identify Nyquist diagrams. These prove that a charge transfer process refers to Cu metal disintegration [24]. In Figure (10), the matching circuit for Cu and electrolyte is established. Table 6 lists the EIS parameters as well as the percent IE. The impedance coefficients for Cu in 2M nitric acid in the presence and absence of an adjusted dosage of ETD were obtained. Figures 8 & 9 indicate the low-frequency area, where the impedance values grow in the presence of ETD compared to the absence of ETD. The radius of the circle rises as the concentration of ETD rises, and therefore the charge transfer resistance in corrosion reactions rises. As a result of the adsorption of the ETD at the Cu/solution contact [28], a high resistance has been produced. CPE parameter (Y_0 and n) is defined in the next balance to estimate the interfacial capacitance C_{dl} data:

$$C_{dl} = Y_0(\omega_{max})^{n-1} \quad (12)$$

where Y_0 is the CPE magnitude, and n is the variance CPE data of the: -1 < n < 1.

Using equation 12, Table 7 shows a decrease in C_{dl} values as ETD dose increases, which can be explained by a decrease in the local dielectric constant and/or an increase in the thickness of the electrical double layer [29]. This is due to ETD molecules adsorbing on the Cu/interface of the solution and generating a protective coating on the Cu solution's interface. Table 7 lists the values of parameters like R_s, R_{ct}, by EIS fitting as well as the derived parameters C_{dl} and IE %.

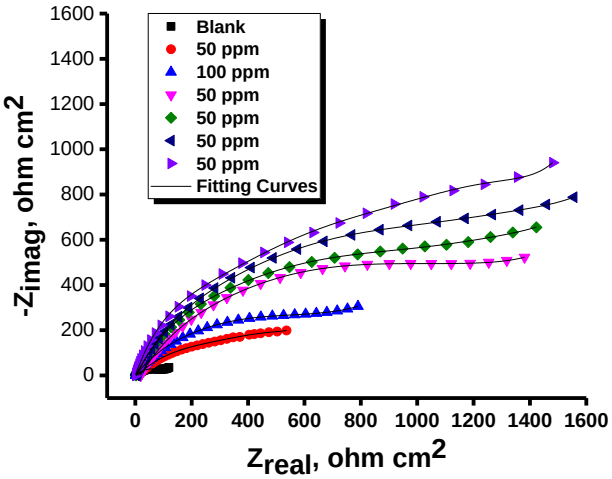

Figure 8. The Nyquist bends for Cu liquefaction in existence and the nonexistence of ETD.

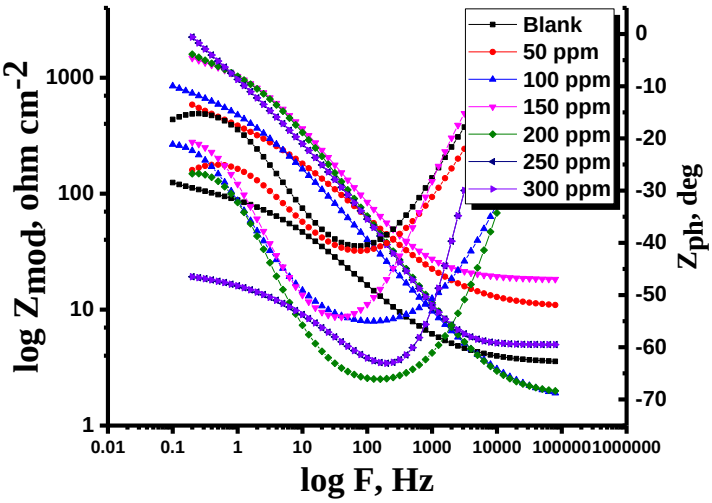

Figure 9. The Bode diagram for Cu dissolution in the existence and absence of ETD**.**

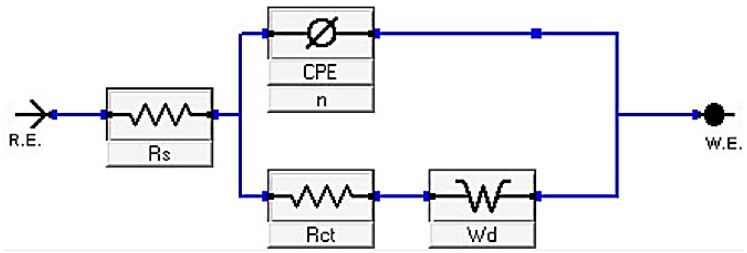

Figure 10. Simple circuit utilized to fit the EIS outcomes.

Table 7. Results from EIS for the liquefaction of Cu in 2.0 M nitric acid at an altered dose of ETD.

[C_{inh}] (ppm)	Y_o, ($\mu\ \Omega^{-1}\ s^n\ cm^{-2}$) x$10^{-6}$	n	Rct, ohm cm^2	Cdl, $\mu F\ cm^{-2}$	Θ	% IE
2 M HNO_3	995	0.664	100	310	--	--
50	462	0.642	447	191	0.776	77.6
100	354	0.659	780	182	0.872	87.2
150	219	0.728	1172	132	0.915	91.5
200	187	0.780	1320	126	0.924	92.4
250	101	0.777	1462	112	0.932	93.2
300	99	0.882	1585	77	0.937	93.7

3.6. Morphology of the surface.

3.6.1. AFM examination.

AFM is a remarkable technology for obtaining high-resolution surface roughness measurements. AFM measurements can provide a wealth of information about Cu surface shape, which aids in understanding the corrosion process. Figure 11 depicts three-dimensional AFM images.

Table 8 summarizes the roughness calculated from the AFM picture. The roughness increased with the addition of HNO_3 due to corrosion on the Cu surface but decreased with the addition of the produced solution [30].

3.6.2. FTIR spectra.

The adsorption of ETD on the Cu surface was confirmed by FTIR. The FT-IR can be used to determine the type of chemical components adsorbed on the surface by analyzing surface variations. The stretching vibration of the O-H stretch corresponds to the peak at 3343 cm^{-1}. This peak was modified to 3355 cm^{-1} in the spectrum of the sample collected from the metal surface. Several ETD peaks in Figure 13 have been modified or vanished, indicating the

presence of bonds between the ETD nitrogen and oxygen atoms and approving the presence of an adsorbed ETD layer on the metal surface.

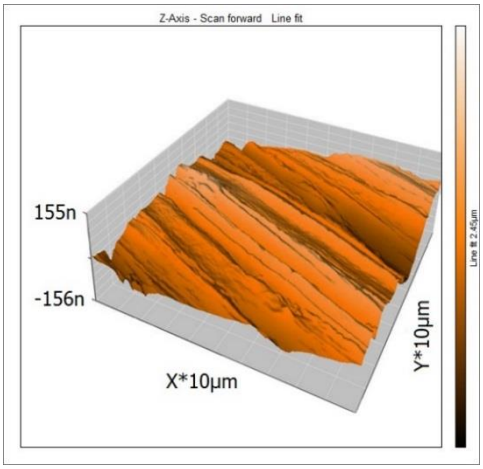

(a) Free

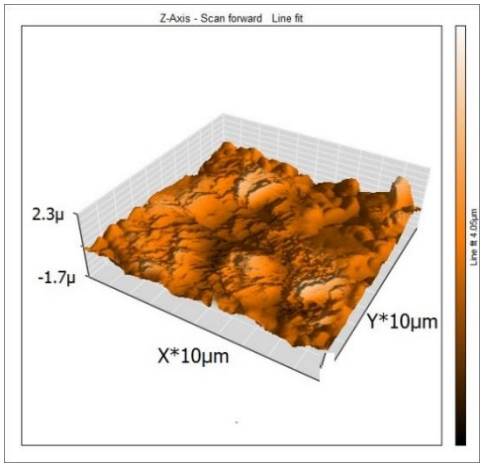

(b) Blank

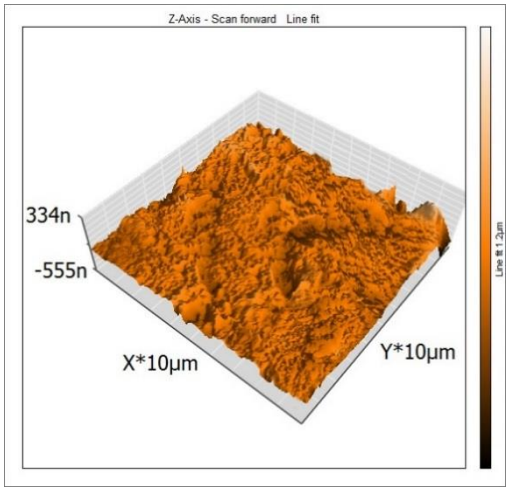

(c) Inhibitor

Figure 11. (**a**) 3D AFM of polished Cu; (**b**) 3D AFM of Cu immersed 2M HNO_3 for 1day; (**c**) 3D AFM image of Cu immersed in 2M HNO_3+300 ppm of ETD for 1 day.

Table 8. AFM parameters of ETD at 25ºC.

Sample	Roughness average (Sa), nm
Free	49
Blank	272
ETD	146

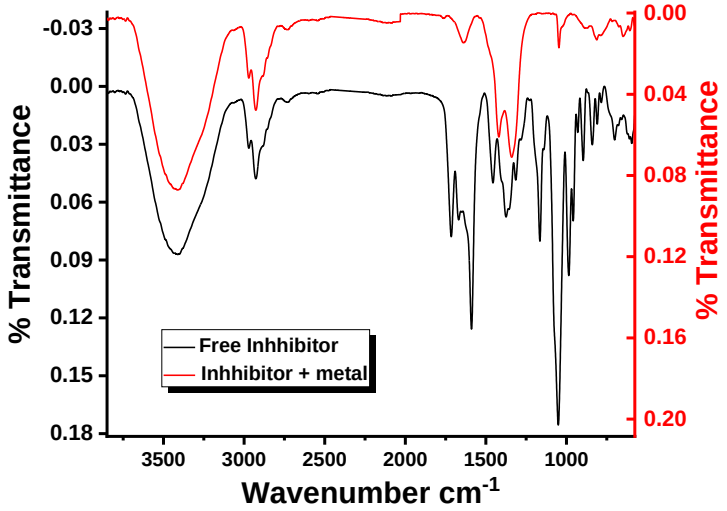

Figure 12. (a) FTIR spectra for free ETD, and (b) FTIR spectra of metal with ETD.

3.6.3. XPS.

The inhibitory layer of ETD on the Cu surface in 2M HNO3 proves that ETD is adsorbed on the Cu surface. Figure 13 depicts the XPS decomposition spectra for each element identified in the surface layer created in a solution that regulates the presence of ETD composition.

Table 9. The binding energies (eV) determination for the large core lines noticed for the surface of Cu which handled by ETD.

Core element	2M HNO_3 + 300 ppm of ETD	
	BE, eV	**Assignments**
C 1s	283.51 286.32 288.21	C-H, C-C, C-O, C+-O
Cu 2p	935.16	Cu_2O
O 1s	530.78 531.73 530.54	Cu_2O, Cu $(OH)_2$
N 1s	398.55	Cu-Nx

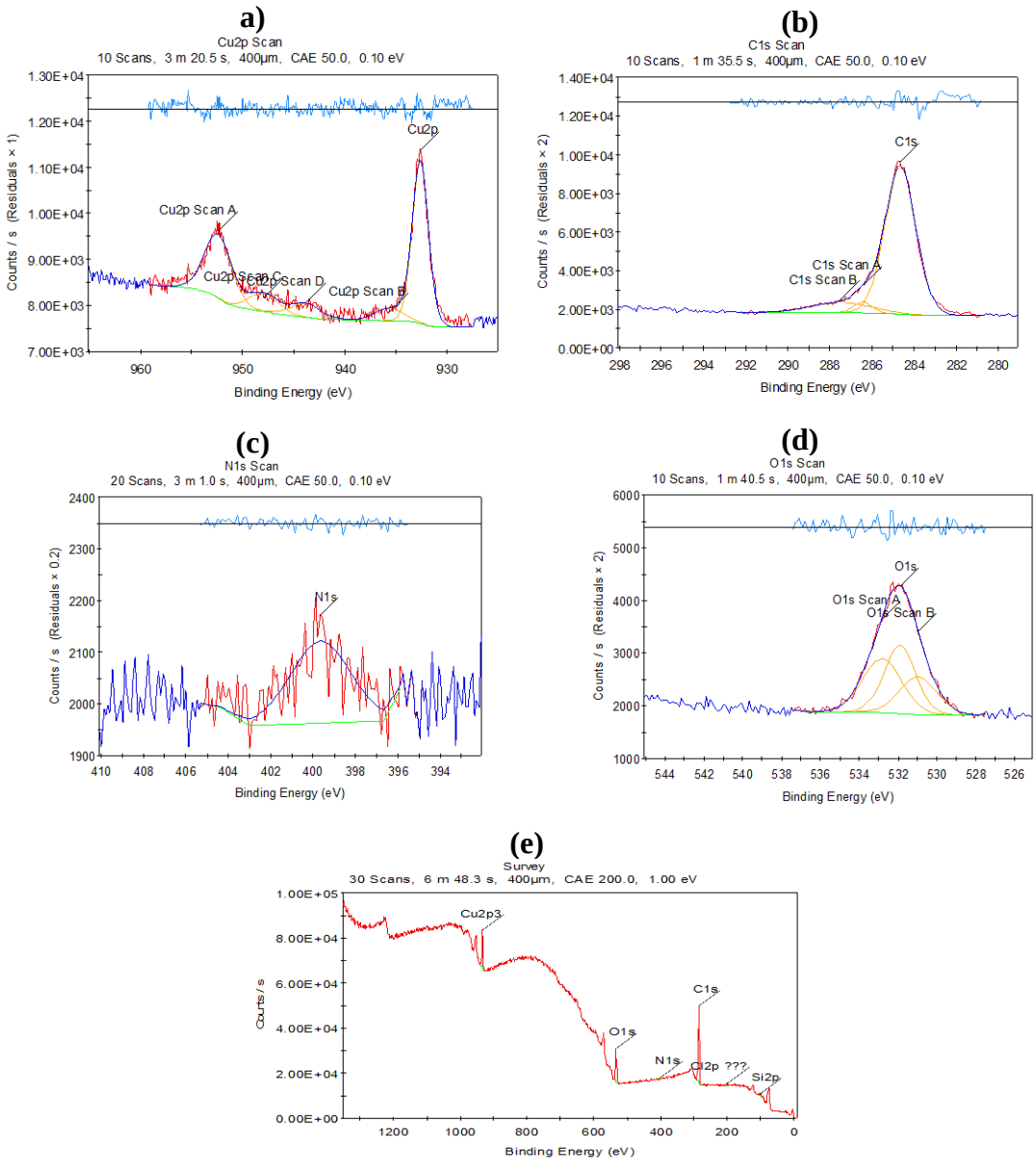

Figure 13. Photoelectric X-rays outcomes from (**a**) Cu 2p; (**b**) C 1s; (**c**) Cl 2p; (d) O 1s; and (**e**) Scanning elements for Cu at 2M nitric acid solutions with 300 ppm from ETD.

We can explain all the spectra in figure by referring to published papers on the interpretation of spectral XPS superficial films, as well as the primary bond energies indicated in Figure 13. The Cu metal spectra recorded when immersed in a 2M HNO_3 containing the highest doses of ETD (300 ppm) were for Cl 2p, Cu 2p, O 1s, and C1s. Table 9 shows the binding energies data (BE, eV) and the same assignment for every peak component [31].

3.7. Mechanism of corrosion inhibition

The inhibitor adsorption on the Cu surface dipped in aqueous HNO_3 is part of the inhibition mechanism. Organic molecules may be found at the metal–solution contact in four different types of adsorptions [32]. From the observations drawn from the altered tests, corrosion hindrance of Cu in 2 M HNO_3 solutions by ETD as chosen from ML, PP, and EIS tests were found to rely on the dose and the nature of the inhibition. The ETD component may protonate in the acid medium. So, there is difficult for these protonated molecules to adsorb on the positive Cu surface [33]. Nitrate ions get first adsorbed on Cu surface, the Cu surface becomes negatively charged, and then the protonated ETD molecules get adsorbed on the nitrated layer as shown below, forming a physisorption mechanism (scheme 1):

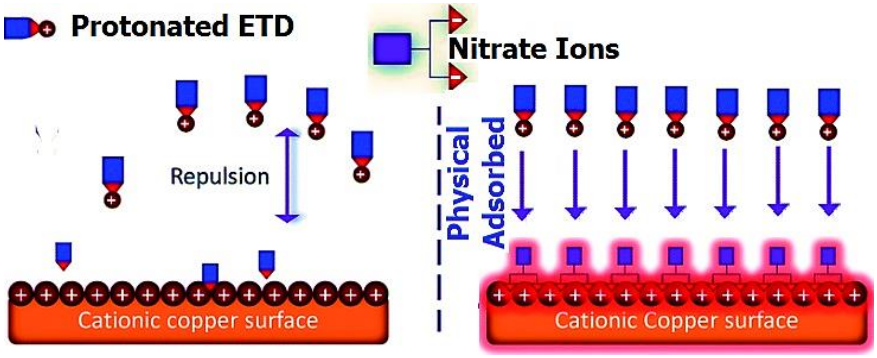

Scheme 1. Mode of adsorption of ETD molecules on Cu surface.

4. Conclusions

The examined ETD in 2.0 M HNO_3 solution can be utilized as effective corrosion protection for Cu. This ETD has an inhibition capacity of 93.5 percent. The percentage of %IE rises by improving ETD dose and lesser temperature. This suggests that ETD being studied are physically adsorbed. The adsorption of ETD had been found to be obeying Langmuir. The adsorption negative free energy ($-\Delta G°_{ads}$) suggests fast and spontaneous adsorption of the ETDs on the surface of Cu, and physisorption was found to be the adsorbed of the ETD. Tafel constant values (βa and βc) confirm the ETD is a mixed type. The AFM, FT-R, and XPS morphology of the adsorbed protective coating on the Cu surface has confirmed the ETD high output of inhibitive action. This research reveals that this ETD is an effective, environmentally friendly, and low-cost inhibitor.

Funding

This research received no external funding.

Acknowledgments

All our gratitude to the anonymous referees for their careful reading of the manuscript and valuable comments that helped shape this paper to the present form. We thank all laboratory

staff of corrosion chemistry from the University of Mansoura (Egypt) for their kind cooperation.

Conflicts of Interest

The authors declare no conflict of interest.

References

1. Vargas, I. T.; Fischer, D. A.; Alsina, M. A.; Pavissich, J. P.; Pastén, P. A.; Pizarro, G. E. Copper corrosion and biocorrosion events in premise plumbing. *Materials* **2017**, *10*, 1036-1056. https://doi.org/10.3390/ma10091036.
2. Wang, Z.; Wang, T.; Zhu, J.; Wei, L.; Shen, Y.; Li, N.; Hu, J. Synergistic effect and mechanism of copper corrosion inhibition using cinnamaldehyde and vanillin in HCl solution: an experimental and theoretical approach. *Colloids and Surfaces A: Physicochemical and Engineering Aspects* **2019**, *563*, 246-254, https://doi.org/10.1016/j.colsurfa.2018.12.012.
3. Vinod, R.; Jobi Thomas, K.; Shaju, S.; Paul, A. A. Corrosion inhibition investigations of 3-acetylpyridine semicarbazone on carbon steel in hydrochloric acid medium. *Res. Chem.* **2014**, *40*, 2689–2701, https://doi.org/10.1007/s11164-013-1122-3.
4. Alibakhshi, E.; Ramezanzadeh, M.; Haddadi, S.A.; Bahlakeh, G.; Ramezanzadeh, B.; Mahdavian, M. Persian Liquorice extract as a highly efficient sustainable corrosion inhibitor for mild steel in sodium chloride solution. *Journal of cleaner production* **2019**, *210*, 660-672, https://doi.org/10.1016/j.jclepro.2018.11.053.
5. de Souza, F.S.; Giacomelli, C.; Gonçalves, R.S.; Spinelli, A. Adsorption behavior of caffeine as a green corrosion inhibitor for copper. *Materials Science and Engineering C* **2012,** *32*, 2436-2444, http://dx.doi.org/10.1016/j.msec.2012.07.019.
6. Lu, Y.; Zhou, L.; Tan, B.; Xiang, B.; Zhang, S.; Wei, S.; Wang, B.; Yao, Q. Two common antihistamine drugs as high-efficiency corrosion inhibitors for copper in 0.5 M H_2SO_4. *Journal of the Taiwan Institute of Chemical Engineers* **2021**, *123*, 11-20, https://doi.org/10.1016/j.jtice.2021.05.027.
7. Li, H.; Zhang, S.; Tan, B.; Qiang, Y.; Li, W.; Chen, S.; Guo, L. Investigation of Losartan Potassium as an eco-friendly corrosion inhibitor for copper in 0.5 M H_2SO_4. *Journal of Molecular Liquids* **2020**, *305*, 112789. https://doi.org/10.1016/j.molliq.2020.112789.
8. Samide, A.; Tutunaru, B.; Dobriţescu, A.; Ilea, P.; Vladu, A-C.; Tigae, C. Electrochemical and theoretical study of metronidazole drug as inhibitor for copper corrosion in hydrochloric acid solution. *Int. J. Electrochem. Sci.* **2016**, *11*, 5520 – 5534, http://dx.doi.org/10.20964/2016.07.67.
9. Feng, L.; Zhang, S.; Tao, B.; Tan, B.; Xiang, B.; Tian, W.; Chen, S. Two novel drugs as bio-functional inhibitors for copper performing excellent anticorrosion and antibacterial properties. *Colloids and Surfaces B: Biointerfaces* **2020**, *190*, 110898, https://doi.org/10.1016/j.colsurfb.2020.110898.
10. Fouda, A. S.; Gadow, H. E. Streptoquin and Septazole: Antibiotic drugs as corrosion inhibitors for copper in aqueous solutions. *Global Journal of Research In Engineering* **2014**, *14*, 21-36.
11. Fouda, A. S.; Abdel-Latif, E.; Helal, H. M.; El-Hossiany, A. Synthesis and Characterization of Some Novel Thiazole Derivatives and Their Applications as Corrosion Inhibitors for Zinc in 1 M Hydrochloric Acid Solution. *Russian Journal of Electrochemistry* **2021**, *57*, 159-171, https://doi.org/10.1134/S1023193521020105.
12. Fouda, A. S.; Abd El-Ghaffar, M. A.; Sherif, M. H.; Taher El-Habab, A.; A. El-Hossiany. Novel anionic 4-tert-octyl phenol ethoxylate phosphate surfactant as corrosion inhibitor for C-steel in acidic media**.** *Prot. Met. Phys. Chem. Surf.* **2020,** *56*, 189-201, https://doi.org/10.1134/S2070205120010086.
13. Fouda, A. S.; El-Hossiany, A.; Ramadan, H. Corrosion Inhibition of Rumex Vesicarius Extract on Stainless Steel 304 in Hydrochloric Acid Solution. *IJRASET* **2017**, *5*, 1698-1710.
14. Fouda, A. S.; El-Hossiany, A. A.; Ramadan, H. M. Calotropis procera plant extract as green corrosion inhibitor for 304 stainless steel in hydrochloric acid solution. *Zaštita materijala* **2017**, *58*, 541-555, http://dx.doi.org/10.5937/ZasMat1704541F.
15. Fouda, A.S.; Motaal, S.M.A.; Ahmed, A.S.; Sallam, H.B.; Ezzat, A.; El-Hossiany, A. Corrosion Protection of Carbon Steel in 2M HCl Using *Aizoon canariense* Extract. *Biointerface Res Appl Chem.* **2022**, *12*, 230-243, https://doi.org/10.33263/BRIAC121.230243.
16. Fouda, A.S.; El-Gharkawy, E.S.; Ramadan, H.; El-Hossiany, A. Corrosion resistance of mild steel in

hydrochloric acid solutions by *Clinopodium acinos* as a green inhibitor. *Biointerface Res Appl Chem*. **2021**, *11*, 9786-9803, https://doi.org/10.33263/BRIAC112.97869803.
17. Fouda, A.S.; Ahmed, R.E.; El-Hossiany, A. Chemical, Electrochemical and Quantum Chemical Studies for Famotidine Drug as a Safe Corrosion Inhibitor for α-Brass in HCl Solution. *Protection of Metals and Physical Chemistry of Surfaces* **2021**, *57*, 398-411, https://doi.org/10.1134/S207020512101010X.
18. Fouda, A.S.; Al-Hazmi, N.E.; El-Zehry, H.H.; El-Hossainy, A. Electrochemical and Surface Characterization of *Chondria Macrocarpa* Extract (CME) as Save Corrosion Inhibitor for Aluminum in 1M HCl Medium. *J Appl Chem*. **2020**, *9*, 362-381.
19. Elgyar, O. A.; Ouf, A. M.; El-Hossiany, A.; Foud, A. S. The Inhibition Action of *Viscum Album* Extract on the Corrosion of Carbon Steel in Hydrochloric Acid Solution. *Biointerface Res Appl Chem.* **2021**, *11*, 14344-14358, https://doi.org/10.33263/BRIAC116.1434414358.
20. Fouda, A.S.; Shalabi, K.; E-Hossiany, A. Moxifloxacin antibiotic as green corrosion inhibitor for carbon steel in 1 M HCl. *Journal of Bio-and Tribo-Corrosion* **2016**, *2*, 18, https://doi.org/10.1007/s40735-016-0048-x.
21. Fouda, A.S.; Rashwan, S.; El-Hossiany, A.; El-Morsy, F. E. Corrosion Inhibition of Zinc in Hydrochloric Acid Solution using some organic compounds as Eco-friendly Inhibitors. *JCBPS* **2019,** *9*, 001-024, https://doi.org/10.24214/jcbps.A.9.1.00124.
22. Fouda, A.S.; Abd El-Maksoud, S.A.; El-Hossiany, A.; Ibrahim, A. Corrosion Protection of Stainless Steel 201 in Acidic Media using Novel Hydrazine Derivatives as Corrosion Inhibitors. *Int. J. Electrochem. Sci*. **2019,** *14*, 2187-2207, https://doi.org/10.20964/2019.03.15.
23. Appa Rao, B.V.; Narsihma Reddy, M. Formation, characterization and corrosion protection efficiency of self-assembled 1-octadecyl-1H-imidazole films on copper for corrosion protection. *Arabian Journal of Chemistry* **2017**, *10*, S3270-S3283, https://doi.org/10.1016/j.arabjc.2013.12.026.
24. El-Tantawy, M.I.; Gadow, H.S.; Rashed, I.G.; Fouda, A.S. Inhibition of Copper Corrosion by Rice Straw Extract in 2M Solution of Nitric Acid, *Biointerface Research in Applied Chemistry* **2022**, *12*, 83 – 104, https://doi.org/10.33263/BRIAC121.083104.
25. Habibiyan, A.; Ramezanzadeh, B.; Mahdavian, M.; Kasaeian, M. Facile size and chemistry-controlled synthesis of mussel-inspired bio-polymers based on Polydopamine Nanospheres: Application as eco-friendly corrosion inhibitors for mild steel against aqueous acidic solution. *Journal of Molecular Liquids* **2020**, *298*, 111974, https://doi.org/10.1016/j.molliq.2019.111974.
26. Fouda, A.S.; El-Dossoki F. I.; El-Hossiany, A.; Sello, E. A. Adsorption and Anticorrosion Behavior of Expired Meloxicam on Mild Steel in Hydrochloric Acid Solution. *Surface Engineering and Applied Electrochemistry* **2020**, *56*, 491-500, http://dx.doi.org/10.3103/S1068375520040055.
27. Fouda, A.S.; Abd El-Maksoud, S.A.; Belal, A.A.M.; El-Hossiany, A.; Ibrahim, A. Effectiveness of Some Organic Compounds as Corrosion Inhibitors for Stainless Steel 201 in 1M HCl: Experimental and Theoretical Studies. *Int. J. Electrochem. Sci.* **2018,** *13*, 9826-9846, https://doi.org/10.20964/2018.10.36.
28. Soltani, N.; Tavakkoli, N.; Attaran, A.; Karimi, B.; Khayatkashani, M. Inhibitory effect of *Pistacia khinjuk* aerial part extract for carbon steel corrosion in sulfuric acid and hydrochloric acid solutions. *Chemical Papers* **2020**, *74*, 1799-1815, https://doi.org/10.1007/s11696-019-01026-y.
29. Fouda, A.S.; Abd El-Maksoud, S.A.; El-Hossiany, A.; Ibrahim, A. Evolution of the Corrosion-inhibiting Efficiency of Novel Hydrazine Derivatives against Corrosion of Stainless Steel 201 in Acidic Medium. *Int. J. Electrochem. Sci.* **2019,** *14*, 6045-6064, https://doi.org/10.20964/2019.07.65.
30. Fouda, A.S.; Eissa, M.; El-Hossiany, A. Ciprofloxacin as Eco-Friendly Corrosion Inhibitor for Carbon Steel in Hydrochloric Acid Solution. *Int. J. Electrochem. Sci.* **2018,** *13*, 11096-11112, https://doi.org/10.20964/2018.11.86.
31. Hsissou, R.; Abbout, S.; Berisha, A.; Berradi, M.; Assouag, M.; Hajjaji, N.; Elharfi, A. Experimental, DFT and molecular dynamics simulation on the inhibition performance of the DGDCBA epoxy polymer against the corrosion of the E24 carbon steel in 1.0 M HCl solution. *Journal of Molecular Structure* **2019**, *1182*, 340-351, https://doi.org/10.1016/j.molstruc.2018.12.030.
32. Fouda, A.S.; Abdel Azzem, M.; Mohamed, S.A., El-Hossiany, A.; El-Desouky, E. Corrosion Inhibition and Adsorption Behavior of Nerium Oleander Extract on Carbon Steel in Hydrochloric Acid Solution. *Int. J. Electrochem. Sci*. **2019,** *14*, 3932-3948, https://doi.org/10.20964/2019.04.44.
33. Motawea, M. M.; El-Hossiany, A.; Fouda, A.S. Corrosion Control of Copper in Nitric Acid Solution using Chenopodium Extract. *Int. J. Electrochem. Sci.* **2019,** *14*, 1372-1387, https://doi.org/10.20964/2019.02.29.